Progress In Electromagnetics Research M, Vol. 86, 125–134, 2019

Efficient High-Speed Strip-Mode SAR Raw Signal Simulator of Extended Scene Included Static and Moving Targets

Liang Yang*

Abstract—In high-speed strip-mode Synthetic Aperture Radar (SAR), the motion between the radar and moving targets during the pulse duration must be considered; however, the existing SAR raw data simulator is unable to handle the case of the moving targets for high-speed SAR exactly. As for the issue, an accurate Point Target Reference Spectrum (PTRS) of the moving targets for high-speed SAR is first derived in the paper, which considers the motion. Further, an accurate and efficient extended scene generator for high-speed SAR included static and moving targets is proposed according to the spectrum. Finally, point targets and extended scene are performed to validate the proposed approach, and its computational complexity is analyzed.

1. INTRODUCTION

Synthetic Aperture Radar (SAR) is a well-established remote sensing instrument in all weather conditions and day and night [1]. The SAR raw data generator is required to the evaluation of focusing algorithms, moving target analysis, and hardware design. The time domain simulator can achieve a realistic simulation, but it is highly time consuming [2]. The frequency domain simulator is put forward to increase the efficiency [3–6], which takes the spatial variant range-azimuth coupling into count and even considers the trajectory deviations of the radar [7, 8]. Moreover, some simulators can generate raw signal of the extended scene included static and moving targets [9–11].

Most pulse radar simulators are based on the "stop-go" approximation. However, under certain circumstances, using the "stop-go" approximation may result in intolerable error. Moreover, with the increasing resolution for SAR imaging from high-speed platforms (space-borne SAR and others), the error would not only lead to localization deviation but also affect focusing [12]. Thus, in high-speed SAR, the motion between the radar and moving targets during the pulse duration must be taken into consideration. As for above issues, in this letter an accurate Point Target Reference Spectrum (PTRS) of the moving targets for high-speed SAR is first derived which takes the motion into account and an accurate and efficient extended scene simulator for high-speed SAR contained static and moving targets is proposed according to the spectrum.

The letter is organized as follows. Section 2 presents the theory of the proposed raw signal simulation approach in high-speed SAR configuration. Section 3 introduces the procedure of the proposed simulator. In Section 4, the simulator is validated by both point target and extended scene simulations. The efficiency is analyzed in Section 5. Conclusions are reported in Section 6.

2. GEOMETRY CONFIGURATION AND 2-D SIGNAL SPECTRUM

In this section, the paper introduces the geometric configuration of the SAR working process, then proposes an accurate echo model, and finally based on the accurate echo model, the accurate frequency domain expression of the echo is introduced using the Principle of Stationary Phase (POSP).

Received 9 August 2019, Accepted 23 October 2019, Scheduled 19 November 2019
* Corresponding author: Liang Yang (yangliang_mail@163.com).
The author is with School of Information and Electrical Engineering, Ludong University, Yantai 264025, China.

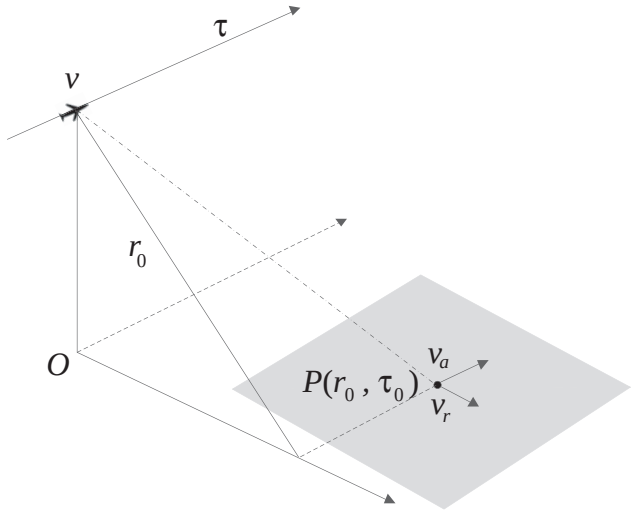

Figure 1. Geometry of the SAR system.

The SAR geometric configuration is shown as Figure 1. In this figure, O stands for the start point; τ represents the slow time; v is the SAR platform velocity. A target denoted by $P(r_0, \tau_0)$ is located in the static scene with velocity v_r in the slant range direction and v_a in the azimuth direction. In this letter, v_r and v_a are assumed to be fixed during the data acquisition, the closest slant range from the platform to the point target $P(r_0, \tau_0)$ is r_0.

According to Figure 1, the slant range of the radar antenna phase center to the ground target can be expressed as

$$R(\tau) = \sqrt{[r_0 + v_r(\tau - \tau_0)]^2 + (v - v_a)^2(\tau - \tau_0)^2} \tag{1}$$

In order to obtain the target echo delay, the two-way distance of the echo needs to be considered. In the conventional pulsed SAR, since the pulse width is very short and platform velocity is slow in the transmission, the movement of the antenna platform during pulse transmission and reception is negligible. i.e., "stop-go" approximation. And the echo delay at this time is double one-way slant delay, which can be expressed as $\tau_d = 2R(\tau)/c$, c is the speed of light. However, in the high-speed platform SAR, the motion between the radar and moving targets during the pulse duration cannot be ignored. Thus, the antenna platform and target motion need to be considered within a short distance in the derivation of the slope course representation.

In order to describe the slant range model of high-speed SAR more vividly, Figure 2 shows the slope geometry model. In the light of Figure 2, the slant range at azimuth time τ is shown in (1) and $\tau + \tau_d$ can be expressed as

$$R(\tau + \tau_d) = \sqrt{[r_0 + v_r(\tau + \tau_d - \tau_0)]^2 + (v - v_a)^2(\tau + \tau_d - \tau_0)^2} \tag{2}$$

where τ_d is the propagation delay that can be determined by

$$\tau_d = \frac{R(\tau) + R(\tau + \tau_d)}{c} \tag{3}$$

Solving τ_d with Eqs. (1)–(3) yields

$$\tau_d = 2\alpha_0 \left[\frac{R(\tau)}{c} + \beta_0(\tau - \tau_0) + \frac{r_0 v_r}{c^2} \right] \tag{4}$$

where α_0 is defined as the Doppler factor, which is expressed as $\alpha_0 = 1/(1 - \beta_0)$ with $\beta_0 = \frac{v_r^2 + (v - v_a)^2}{c^2}$.

Assume that the received baseband signal from a point target $P(r_0, \tau_0)$ is

$$S_0(\tau, t, \tau_0, r_0) = \sigma(\tau_0, r_0) \exp\left[-j2\pi f_0(t - \tau_d)\right] \exp\left[j\pi K_r(t - \tau_d)^2\right] \tag{5}$$

where $\sigma(\tau_0, r_0)$ is the reflectivity coefficient of the point target; t represent the range time variables, f_0 is the carrier frequency; K_r stands for the chirp rate.

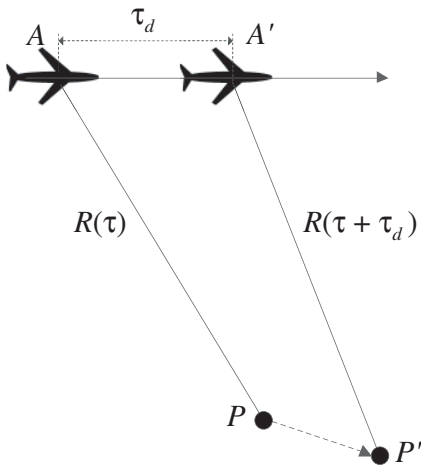

Figure 2. Transmit and receive timing considering the platform movement.

Using Fourier Transform (FT) with respect to range time

$$S_0(\tau, f_t, \tau_0, r_0) = \int S_0(\tau, t, \tau_0, r_0) \exp\left[-j2\pi f_t t\right] dt \tag{6}$$

Using POSP we can obtain

$$S_0(\tau, f_t, \tau_0, r_0) = \sigma(\tau_0, r_0) \exp\left[-j\pi f_t^2 / K_r\right] \exp\left[-j2\pi(f_0 + f_t)\tau_d\right] \tag{7}$$

where f_t denotes the range frequency. In order to obtain the 2-D spectrum, a further Fourier transformation to the azimuth time is performed.

$$S_0(f_\tau, f_t, \tau_0, r_0) = \int S_0(\tau, f_t, \tau_0, r_0) \exp\left[-j2\pi f_\tau \tau\right] d\tau \tag{8}$$

Calculating the point of stationary phase τ_d by the POSP yields

$$\tau = \tau_0 - \frac{R_0 v_r}{v_{eq}^2} - \frac{r_0 \alpha \beta}{v_{eq}\sqrt{1-\beta^2}} \tag{9}$$

where α is defined as the velocity modulation factor calculated by $\alpha = \sqrt{1-(v_r/v_{eq})^2}$ and $\beta = cf_\tau / 2\alpha_0 v_{eq}(f_0 + f_t) + v_{eq}/c$ with $v_{eq} = \sqrt{v_r^2 + (v - v_a)^2}$.

The accurate 2-D spectrum of the high-speed platform SAR included moving target is expressed as

$$S_0(f_\tau, f_t, \tau_0, r_0) = \sigma(\tau_0, r_0) \times \exp\left[-j\Phi(f_\tau, f_t)\right] \tag{10}$$

where

$$\begin{aligned}\Phi(f_r, f_\tau, r_0) \;=\; & \frac{4\pi r_0 \alpha_0 \alpha}{c} \sqrt{(f_0 + f_t)^2 - \left[\frac{v_{eq}}{c}(f_0 + f_t) + \frac{c f_\tau}{2\alpha_0 v_{eq}}\right]^2} \\ & - \frac{4\pi \alpha_0 f_t r_0 v_r}{c^2} - \frac{2\pi r_0 v_r f_\tau}{v_{eq}^2} + \frac{4\pi \alpha_0 f_0 r_0 v_r}{c^2} + \frac{\pi \left(f_t - f_\tau\right)^2}{K_r} + 2\pi f_\tau \tau_0 \end{aligned} \tag{11}$$

and f_τ is the azimuth frequency.

The following are some remarks to make clear of the general PTRS of the moving targets for high-speed SAR in (11).

(1) When the velocities of moving targets are both equal to zero, Eq. (11) is the same as Eq. (27) in [13].

(2) The first term is the range and azimuth coupling, and compared with the PTRS of the fixed targets, the coupling term of the moving target is affected by the velocity modulation factor. Therefore, the moving target will appear bearing defocus and a slight distance offset on the SAR image.

(3) The second term is the range shift of high-speed SAR, which is induced by the motion during the pulse duration in the range.

(4) The third term is the azimuth displacement caused by the range velocity. Compared to the traditional expression of the azimuth displacement of the pulsed SAR, the azimuthal displacement in the high-speed SAR is also related to the equivalent velocity.

(5) The fourth term is the fixed phase owing to the range speed of the moving target.

The remaining terms are the same as the static target.

The paper proposes an efficient extended scene generator for high-speed SAR with static and moving targets in the 2-D frequency domain. The basic steps are outlined as follows in next section.

3. HIGH-SPEED SAR RAW DATA SIMULATION

The high-speed SAR raw signal simulation procedure for the extended scene included fixed and moving target can adopt the method in paper [10] as shown in Fig. 3(a); however, the basic steps of the raw data simulator are not alike because the 2-D spectra of high-speed SAR and non-high-speed SAR are different. The steps of the simulator for the high-speed SAR are shown in Fig. 3(b).

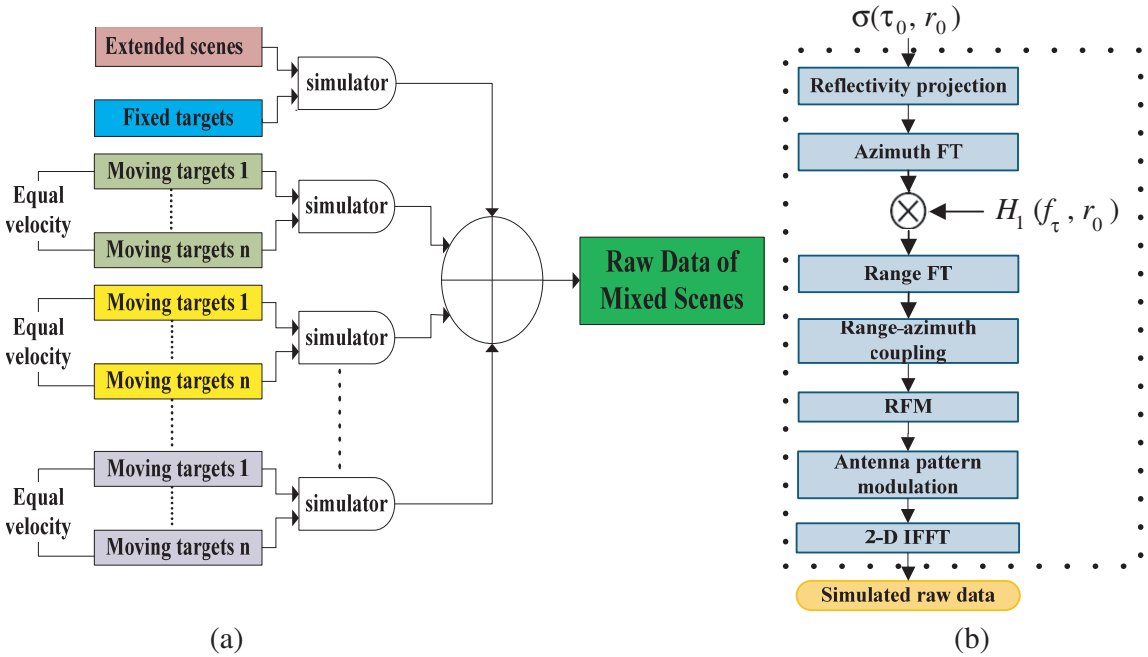

Figure 3. (a) Mixed scenes raw data simulation procedure and (b) flow of the high-speed SAR raw signal simulator.

The basic steps of high-speed SAR raw data simulation are outlined as follows.

(1) The reflectivity $\sigma(\tau_0, r_0)$ is projected to the imaging plane, and the signal is expressed as

$$g(\tau, t) = \iint G_r(t)\sigma(\tau_0, r_0)\delta(\tau - \tau_0)\delta(t - t_0)d\tau_0 dr_0 \tag{12}$$

where $G_r(t)$ represents the range antenna beam pattern, and t_0 is the propagation delay of the interested target corresponding to the one in the scene center, which can be expressed as

$$t_0 = \frac{2\alpha_0\alpha(r_0 - r_{ref})}{c} \tag{13}$$

(2) Performing the Fast Fourier Transform (FFT) in the azimuth direction to transform the signal into the azimuth frequency domain and then compensating the differential azimuth shift caused by range velocities, the signal is given as

$$H_1(r_0, f_\tau) = \exp\left(j\frac{2\pi(r_0 - r_{ref})v_r f_\tau}{v_{eq}^2}\right) \tag{14}$$

Thus, the signal becomes

$$g(f_\tau, t) = \iint G_r(t_0)\sigma(\tau_0, r_0)\,\delta(t - t_0)\exp\left(j\frac{2\pi(r_0 - r_{ref})v_r f_\tau}{v_{eq}^2}\right)\exp(-j2\pi f_\tau\tau_0)\,d\tau_0 dr_0 \tag{15}$$

(3) Computing the range FFT of the scene data, the signal is expressed as

$$g(f_\tau, f_t) = \iint G_r(t_0)\sigma(\tau_0, r_0)\exp(-j2\pi f_\tau\tau_0)\exp(-j2\pi f_t t_0)\exp\left(j\frac{2\pi(r_0 - r_{ref})v_r f_\tau}{v_{eq}^2}\right)d\tau_0 dr_0 \tag{16}$$

(4) The range frequency transition will be performed in the 2-D frequency domain to simulate the range-azimuth coupling, which can be expressed as

$$f_t \to \sqrt{(f_0 + f_t')^2 - \left[\frac{v_{eq}^2}{c}(f_0 + f_t') + \frac{cf_\tau}{2\alpha_0 v_{eq}}\right]^2} - \frac{v_r}{\alpha c}f_t' \tag{17}$$

where f_t' represents the new range frequency.

(5) Reference Function Multiplication (RFM) operation is applied to simulate all the range-invariant phase, thus the function is expressed as

$$H_{\mathrm{RFM}}(f_\tau, f_t') = \exp\left\{\begin{array}{l} -j\dfrac{4\pi\alpha_0\alpha r_{ref}}{c}\sqrt{(f_0 + f_t')^2 - \left[\dfrac{v_{eq}^2}{c}(f_0 + f_t') + \dfrac{cf_\tau}{2\alpha_0 v_{eq}}\right]^2} \\ +j\left(\dfrac{4\pi\alpha_0 f_t' r_{ref} v_r}{c^2} + \dfrac{2\pi f_\tau r_{ref} v_r}{v_{eq}^2}\right) + \dfrac{\pi\left(f_t' - f_\tau\right)^2}{K_r} \end{array}\right\} \tag{18}$$

(6) Add antenna pattern modulation according to $W_a^2 = \left(-\frac{r_0}{v_{eq}}\left(\frac{\alpha\beta}{\sqrt{1-\beta^2}} + \frac{v_r}{v_{eq}}\right) - \frac{f_t}{K_r}\right)$ in the azimuth and rect $\left(\frac{f_t}{B_r}\right)$ in the range, where B_r is the transmitted bandwidth.

(7) After all of the aforementioned operations, the high-speed SAR raw signal can be obtained by applying 2-D Inverse Fast Fourier Transform (IFFT). The simulated signal is expressed as

$$\begin{aligned} g(\tau, t, \tau_0, r_0) \;=\; & \iint \sigma(\tau_0, r_0)G_r(t)G_a(\tau)\mathrm{rect}\left(\frac{t - t_0}{T_r}\right) \\ & \exp\left[-j2\pi f_0(t - \tau_d)\right]\exp\left[j\pi K_r(t - \tau_d)^2\right]dr_0 d\tau_0 \end{aligned} \tag{19}$$

where T_r is the chirp duration.

By taking advantage of FFT, the proposed approach reduces the computational load with respect to the time domain raw data generation. And the raw data of the three types of targets are all accurately simulated with the proposed simulator.

4. SIMULATION AND VALIDATION

In this section, the raw data of moving targets generated with proposed method are verified by both point targets and extended scenes. In order to quantitatively analyze the characteristics of the moving target, we expand the coupling term in Eq. (11) to three items by using Taylor series.

$$\begin{aligned} & \Phi_{\mathrm{Couple}}(f_r, f_\tau, r_0) \\ \approx\; & -\frac{4\pi r_0\alpha_0\alpha}{c}\left[Df_0 + \left(\frac{1 - \mu_1\mu_2}{D} - \frac{v_r}{\alpha c}\right)f_t - \frac{(\mu_1 - \mu_2)^2}{2f_0 D^3}f_t^2 + \frac{(\mu_1 - \mu_2)^2(1 - \mu_1\mu_2)}{2f_0^2 D^5}f_t^3\right] \end{aligned} \tag{20}$$

where $D = \sqrt{1-\mu_1^2}$, $\mu_1 = \frac{v_{eq}}{c} + \frac{cf_\tau}{2\alpha_0 v_{eq} f_0}$, $\mu_2 = \frac{v_{eq}}{c}$.

It can be seen from Equation (20) that the azimuth modulation phase of the moving target is $-\frac{4\pi r_0 \alpha_0 \alpha}{c} D f_0$, which is affected by the moving target distance and azimuth velocity. Therefore, the range velocity will also cause a slight defocusing of the moving target in addition to the target azimuth velocity. The phase causing defocus can be accurately expressed as

$$\Delta\Phi_{\text{smear}}(r_0, f_\tau) = -\frac{4\pi r_0 \alpha_0 \alpha}{c} D f_0 + \frac{4\pi r_0 \alpha_0'}{c} D' f_0 \tag{21}$$

where $D' = \sqrt{1-\mu_1'^2}$.

Based on Eq. (20), the range shifts of moving targets in the final SAR image are computed for comparing. Then, the range shift in the final SAR image can be formulated as

$$Vr = r_0 \alpha_0 \alpha \left(\frac{v_r}{\alpha c} - \frac{1-\mu_1\mu_2}{D} \right) + r_0 \alpha_0' \frac{1-\mu_1'\mu_2'}{D'} \tag{22}$$

where $\mu_1' = \frac{v}{c} + \frac{cf_\tau}{2\alpha_0' v f_0}$, $\mu_2' = \frac{v}{c}$.

The azimuth migration can be directly obtained from the third term in Eq. (11), which is expressed as

$$Vx = r_0 v_r v / v_{eq}^2 \tag{23}$$

In the point targets simulation, the paper verifies the echo simulation of the static point target and moving target, respectively, while the stationary point target, stationary distributed target, and moving distributed target are also analyzed and verified by the extended scene simulation.

4.1. Raw Data Simulation of the Point Target

The static point target is verified by the focus result. The simulation system parameters are shown in Table 1. Figure 4 gives the resulting impulse responses of the static point target, which shows that the static point target is well compressed. Figures 5(a) and (b) compare the impulse response of static point target with respect to the time domain method in the azimuth and range directions, respectively. In Figures 5(a) and (b), we label the proposed method as frequency domain method (FDM) and denote time domain approach as time domain method (TDM). By comparison, we can see that the two methods are basically the same. To quantify the focus performance more specifically, the analysis results containing the impulse response width (IRW), peak side-lobe ratio (PSLR), and integrated side-lobe ratio (ISLR) of the static point target are shown in Table 2. We can see that the measurements of target parameters agree well with the theoretical values. The results validate the effectiveness of the proposed approach.

The paper will measure the azimuth offset and range offset after imaging of moving point targets to verify the effectiveness of the simulator. The moving point target simulation test will compare the three sets of values under the same parameter. The first group is the theoretical value according to Eqs. (22) and (23); the second group is the 2-D offset of the target measured by the echo simulation

Table 1. System parameters.

Parameters	Values
Carrier Frequency	9.6 GHz
Reference Range	800 km
Transmitted Bandwidth	600 MHz
Platform Velocity	7500 m/s
Pulse Repeat Frequency	5000 Hz
Pulse Length	40 μs
Azimuth beam width	0.005 rad
Squint Angle	0°/30°

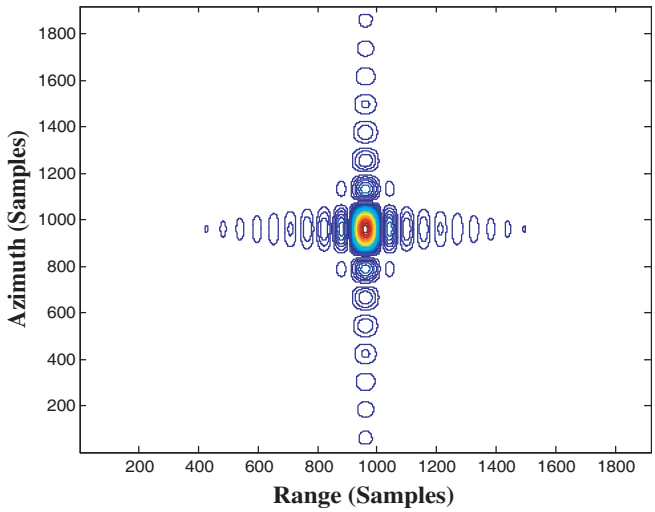

Figure 4. Resulting impulse responses of the static point target.

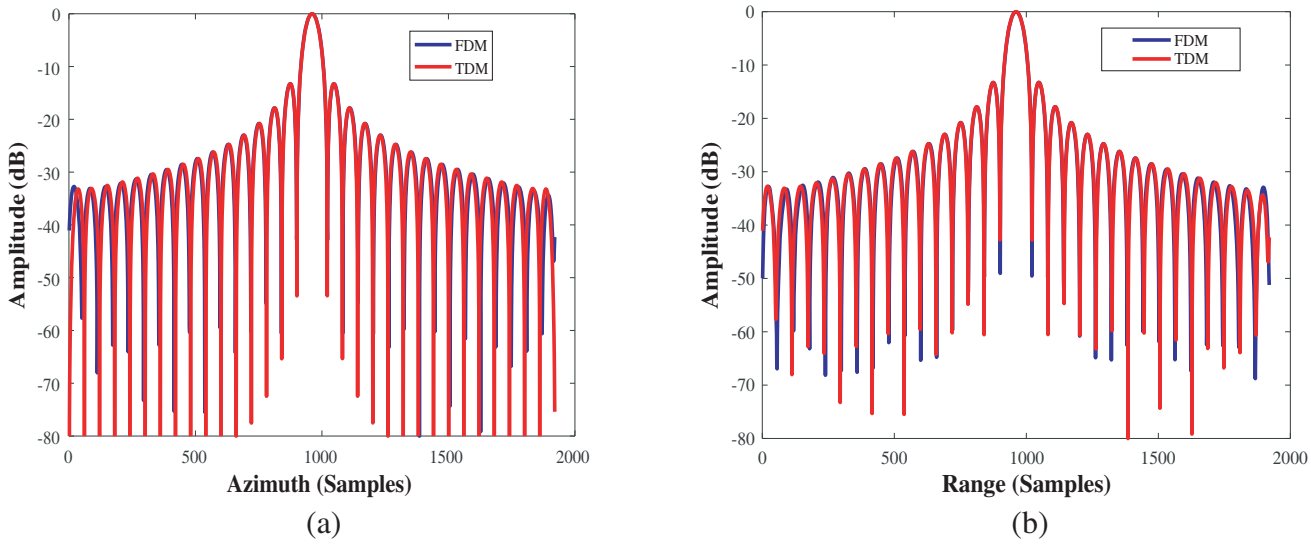

Figure 5. (a) Comparison with the azimuth profiles of the resulting impulse response of static point target of time domain method and (b) comparison with the range profiles of the resulting impulse response of static point target of time domain method.

Table 2. Performance analysis of static point target.

Range			Azimuth		
IRW (m)	PSLR (dB)	ISLR (dB)	IRW (m)	PSLR (dB)	ISLR (dB)
0.96	−13.27	−10.23	0.95	−13.23	−10.19

imaging process using the simulator proposed in this paper (labelled as FD); the third group is the 2-D offset measurement of the target after echo simulation imaging is performed by the time domain method (labelled as TD).

Eight moving point targets with different velocities but the same range are evaluated, and last two

Table 3. Simulation results.

	Target velocities (v_r, v_a) m/s	Azimuth shift (m)			Range shift (m)		
		Theory	FD	TD	Theory	FD	TD
Broadside	(0, 0.5)	0	0.083	0.054	0	0	0
	(0, 1)	0	0.091	0.063	0	0	0
	(0.5, 0)	53.333	53.333	53.336	0.0018	0.0019	0.0018
	(1, 0)	106.667	106.667	106.677	0.0071	0.0076	0.0073
	(0.5, 1)	53.456	53.336	53.303	0.0019	0.0020	0.0019
	(1, 1)	106.712	107.056	106.956	0.0075	0.0080	0.0077
Squint mode	(0.5, 0)	53.325	53.305	53.201	0.0021	0.0029	0.0026
	(1, 0)	106.676	106.432	106.398	0.0082	0.0092	0.0087

of them are configured in squint mode. Table 3 gives the range and azimuth shifts results of moving targets with different velocities but the same range.

In order to better understand the results, some explanations are given as follows.

(1) The deviation of the values in first two moving targets is caused by the approximation of the measurement.

(2) The range velocity not only causes the azimuth of the moving target to shift, but also causes a slight shift in the range direction.

(3) Due to the modulation of the coupling term by the Doppler factor, the azimuth velocity of the target also causes a slight distance and azimuth offset.

(4) Due to the influence of the Doppler center, the distance offset is slightly different from the broadside in the squint mode.

Through the above simulation results, we can see that the proposed method can simulate the echoes of moving targets accurately and efficiently.

4.2. Raw Data Simulation of the Extended Scene

In this subsection, the proposed approach is validated by simulating the high-speed SAR raw signal of a real scene. The real SAR image is used as backscattering coefficients, as shown in Figure 6. There

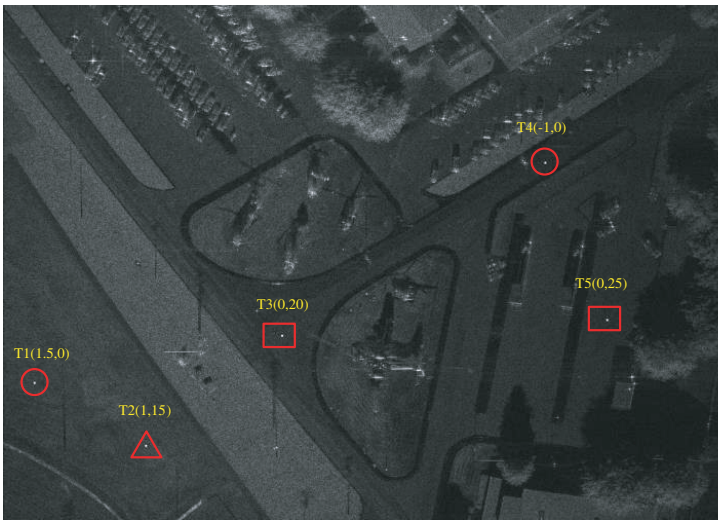

Figure 6. The simulation scene imaging with moving targets data generator.

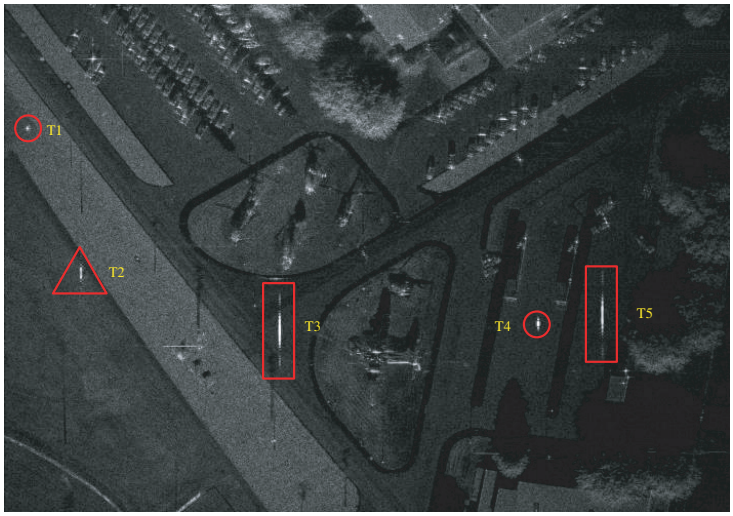

Figure 7. Focus result with raw data generated moving targets by the proposed simulator.

are five moving distributed targets with a size of $6 * 6$ pixels which are artificially added in the scene. The velocities of the targets are labelled in Figure 6 in the form of (v_r, v_a). The raw data of the mixed scene are generated applying the proposed method, and the processed raw data are shown as Figure 7.

Processing the simulated raw signal, a well-focused SAR image is acquired, as shown in Figure 7, without any geometry deviation or defocusing. With regard to the moving targets in the scene, the targets (T1, T4) only with range velocities are migrated in the azimuth direction with a small smear effect; the targets (T3, T5) only with azimuth velocities exhibit a defocused phenomenon; and the target (T2) with range and azimuth velocities generates both effects. The results further validate that the proposed frequency domain approach can accurately simulate the high-speed platform SAR signal included moving targets.

5. COMPUTATIONAL COMPLEXITY ANALYSES

To reveal the efficiency of the presented frequency domain SAR scene simulator included moving targets, the computational complexity of the proposed method is compared with the time domain approach using the complex multiplication.

The computation of the proposed simulator with a single type of target is

$$N_f = 10N_aN_r \log_2(N_aN_r) + 12N_aN_r + 2(2M_{\text{ker}} - 1)N_aN_r \tag{24}$$

where M_{ker} is the length of interpolation kernel. N_a and N_r are the size of generated scenes in the azimuth and range direction, respectively. The computation of the time domain simulator can be expressed as

$$N_t = N_a^2 N_r^2 \tag{25}$$

However, it is tough to assess its efficiency directly because of the employed mixed targets in the proposed simulation. Suppose that in a generated scene, there are $m\%$ targets belonging to moving point target (MPT); $n\%$ are moving distributed target (MDT) with TUS of K; and the remaining are fixed point target (FPT) and fixed distributed target (FDT), then the accelerate ratio of the proposed method can be expressed as

$$\eta = \frac{(m\% * N_aN_r + n\% * N_aN_r/K + 1)N_f}{N_t} \tag{26}$$

Thus, the efficiency of the presented generator is mainly decided by the percentage of moving point and distributed target. However, these targets usually occupy very small portion of the whole generated scene. Therefore, the mixed scene generator is still highly efficient. For example, a simulated scene with

8192 bins in the range direction and in the azimuth direction respectively, in which 0.001% belongs to MPT; 0.02% is MDT with TUS of $30 * 30$; the length of interpolation kernel is 8, then the accelerate ratio of this method is about 323, which greatly increases the efficiency.

6. CONCLUSION

In the paper an efficient and precise high-speed strip-mode SAR raw data simulation approach for extended scene included static and moving targets is proposed. The simulator is based on an analytical slant range model and an accurate 2-D spectrum, which consider the motion of the radar and moving targets during the pulse duration compared to the existing generator. Numerical results demonstrate that the present method can reduce the computational time significantly without accuracy loss while simulating extended scenes contained moving target of high-speed platform SAR raw data.

REFERENCES

1. Curlander, J. and R. Mc Donough, *Synthetic Aperture Radar Systems and Signal Processing*, New York, 1991.
2. De Mori, V. F., "A time-domain raw signal simulator for interferometric SAR," *IEEE Trans. Geosci. Remote Sens.*, Vol. 42, 1811–1817, 2004.
3. Franceschetti, G., M. Migliaccio, D. Riccio, and G. Schirinzi, "SARAS: A synthetic aperture radar (SAR) raw signal simulator," *IEEE Trans. Geosci. Remote Sens.*, Vol. 30, 110–123, 1992.
4. Yang, L., W. D. Yu, S. C. Zheng, and L. Zhang, "Efficient bistatic SAR raw signal simulator of extended scenes," *International Journal of Antenna and Propagation*, Vol. 3, 1–9, 2014.
5. Zhang, F., X. J. Yao, H. Y. Tang, Q. Yin, Y. X. Hu, and B. Lei, "Multiple mode SAR raw data simulation and parallel acceleration for Gaofen-3 mission," *IEEE Journal of Selected Topics in Applied Earth Observations and Remote Sensing*, Vol. 11, 2115–2126, 2018.
6. Martino, G. D., A. Iodice, D. Poreh, and D. Riccio, "Pol-SARAS: A fully polarimetric SAR raw signal simulator for extended soil surfaces," *IEEE Trans. Geosci. Remote Sens.*, Vol. 56, 2233–2247, 2018.
7. Franceschetti, G., A. Iodice, S. Perna, and D. Riccio, "SAR sensor trajectory deviations: Fourier domain formulation and extended scene simulation of raw signal," *IEEE Trans. Geosci. Remote Sens.*, Vol. 44, 2323–2334, 2006.
8. Khwaja, A. S., L. Ferro-Famil, and E. Pottier, "Efficient stripmap SAR raw data generation taking into account sensor trajectory deviations," *IEEE Geosci. Remote Sens. Lett.*, Vol. 8, 794–798, 2011.
9. Dogan. O. and M. Kartal, "Efficient strip-mode SAR raw-data simulation of fixed and moving targets," *IEEE Geosci. Remote Sens. Lett.*, Vol. 8, 884–888, 2011.
10. Yang, L., W. Yu, Y.-H. Luo, and S. Zheng, "Efficient strip-mode SAR raw data simulator of extended scenes included moving targets," *Progress In Electromagnetics Research B*, Vol. 53, 187–203, 2013.
11. Yang, L., W. D. Yu, R. Wang, and Y. H. Luo, "Efficient strip-mode SAR raw signal simulation of mixed targets based on accurate 2-D spectrum," *IEEE Radar Conference*, Canada, 2013.
12. Breit, H., T. Fritz, U. Balss, M. Lachaise, A. Niedermeier, and M. Vonavka, "Terra SAR-X SAR processing and products," *IEEE Trans. Geosci. Remote Sens.*, Vol. 48, 727–740, 2010.
13. Liu, Y., M. D. Xing, G. C. Sun, X. L. Lv, Z. Bao, W. Hong, and Y. R. Wu, "Echo model analyses and imaging algorithm for high-resolution SAR on high-speed platform," *IEEE Trans. Geosci. Remote Sens.*, Vol. 50, 933–950, 2012.